Characterization of Bi-Directional Optical Backplane and Performance Enhancement with Multi-Bus Lines

Gicherl Kim and Ray T. Chen
Microelectronic Research Center
Department of Electrical and Computer Engineering
University of Texas at Austin

Abstract

The concept of a bi-directional optical backplane with multi-bus lines for a high performance system containing multi-chip module (MCM) boards, operating at 850 nm, is introduced. The backplane reported here employs VCSEL arrays and photodetector arrays as transceivers. Optical beams from a transmitter are fanned out by deflectors which are arrays of multiplexed polymer-based waveguide holograms, and then undergo total internal reflection inside a waveguiding plate, and finally reach the target receiver arrays on the edge of boards. We have designed a bi-directional optical backplane for the data communications application in a nine-board system. Packaging related issues such as misalignment, crosstalk and signal to noise ratio have been studied for the reliable system based on the Gaussian beam approximation. By integrating 140μm-pitch (1D) or 250μm-pitch (2D) VCSEL arrays, microlens arrays, and photodetector arrays into our design of backplane, we have demonstrated optical backplane with multi-bus lines and experimentally realized this architecture with 1D and 2D bus lines which greatly increase the bus bandwidth of the backplane. Frequency response of our devices shows a bandwidth of 2.5 THz, which is higher bandwidth. Eye diagrams up to 1.5 GHz have been demonstrated with clear eyes.

1. Introduction

Optical interconnections have been of interest at all levels in digital computers for applications between mainframes, modules, boards, chips and even points within a chip. Optics is ideally suited for implementing these interconnection networks because of its inherent characteristics such as high speed, high spatial bandwidth, low signal crosstalk, and capability of wavelength division (de)multiplexing through common media. Optical backplanes utilize optical signals to realize communication for board to board interconnection; each board is equipped with optoelectronic converter (laser diode and photodetector) for the emission and detection of modulated optical signals. Optical interconnection provides the potential of higher data rate for each bus channel and the advantage of reduced transmission line related effects. In addition, the number of optical fan-outs is not limited by the capacitive loading effects.

In past few years, several optical bus architectures based on the optical backplane concept have been proposed. These architectures include waveguide bus systems[1], substrate-mode guided-wave bus systems implemented with waveguiding plates and holographic coupling elements[2,3], and free-space bus systems implemented through free-space optical interconnections[4].

Although optoelectronics is increasing attractive for backplane applications, difficulties associated with optoelectronic systems, such as misalignment and losses due to transition between optical and electrical signals, preclude the popularity of optics for the interconnection levels. Other efforts in enhancing performance of the backplane are mainly devoted to increasing the bandwidth. The backplane bandwidth is defined as the product of the data bus width and the data rate for each bus channel. Increasing the number of the bus lines can thus greatly multiply the bus bandwidth. There have been several different approaches [5,6] to utilize array devices. However, a number of recent attempts were stimulated by the advances of VCSEL. An attractive feature of VCSEL technology is the capability of being fabricated into uniform, individually addressable, one or two-dimensional arrays[7,8]. Many optical interconnection systems taking advantage of these VCSEL arrays have been developed or manufactured.

In this paper, characteristics of our optical interconnection devices are investigated. Packaging and wavelength instability induced misalignment are studied, and a GRIN lens or microlens are introduced into our system which greatly relaxes the alignment difficulty. The power consumption of the system is considered also and the ranges of allowable laser power input are specified. The bandwidth and data transfer integrity of the device are measured. Finally we report a bi-directional optical backplane with multi-bus lines by integrating VCSEL arrays, lens, and photodetector arrays into our design.

Part of the SPIE Conference on Optoelectronic Interconnects VI
San Jose, California • January 1999
SPIE Vol. 3632 • 0277-786X/99/$10.00

2. Realization of bi-directional optical backplane with multi-bus lines

Current efforts in enhancing the performance of the backplane are mainly devoted to increasing the aggregate bandwidth. Array devices should be used to increase the aggregate bandwidth of a backplane. Although several approaches utilize array devices, the VCSEL as a transmitter array has evolved into efficient and reliable device. By taking advantage of one and two-dimensional VCSEL arrays, employing multiplexed holograms and photodetector arrays, we propose and demonstrate a performance enhanced optical backplane with 1-D and 2-D multi-bus lines.

The previously demonstrated optical bi-directional backplane[3] has only one bus line. By incorporating arrays of transmitter and receiver multichip modules on each side of the waveguiding channel, multi-bus line backplane architecture can easily be constructed as shown in Fig. 1. In this design we utilize the fan-outs directed to the opposite side of the transmitters. This arrangement will result in a simpler transceiver design and ease the system packaging. Although we use the same waveguiding structure provided by the array of multiplexed holograms and the waveguiding plate, the overall design must be changed to integrate with electrical processor/memory boards. The center of one hologram is separated from those of the adjacent ones by 3cm, which is the standard inter-board distance in the electrical backplane environment.

Fig. 1 shows the detailed diagram of the backplane with multi-bus lines using VCSEL and photodetector arrays, and also indicates the necessary components integrated into the transmitter and receiver multichip modules. As there is another set of fan-outs directed to the transmitter modules, optical isolators are included on the transmitter modules to block them. When the guided optical signals are packed closely with each other, crosstalk between the adjacent channels may degrade the performance of the system. The mechanisms contributing to this crosstalk can be due to the misalignment of the adjacent channels, or the spreading of the optical signal spots with propagation distance. All of these finally lead to partial overlap among the optical signals from adjacent channels at the output ports.

The overall architecture employing the design of Fig. 1 is shown in Fig. 2. We can see that the arrangement of the transmitter and the receiver is in a plane perpendicular to the multi-processor/memory boards. Another difference between this design and the previous one is that here the communication and conversion occur at the backside of the backplane while for the previous one, they occur at the interface between the backplane and the boards.

Fig. 3 shows the picture of the VCSEL array we currently use in our lab. The device has a total of 32 VCSELs for 1-D application and 64 VCSELs (8x8) for 2-D application, operating at a wavelength of 0.85 μm. Within the fabrication error, all the VCSELs in the array are identical. The array has 140 μm and 250 pitch, respectively. An output power was measured about 1-2 mW at 10 mA operating current. The experimental curves of current versus voltage and output power versus current in room temperature show a threshold voltage of ~1.5 V and a threshold current of ~4 mA. At a current of ~37 mA, the output from the VCSEL reaches a maximum of ~8.7 mW. After that, the output decreases with the increase of current. The far-field output profiles of the VCSEL are demonstrated in Fig. 4. Fig. 4 (a) is the output profile at a distance of ~1 mm from the emission window, and Fig. 4 (b) is at 5 cm further away from Fig. 4 (a). By measuring the FWHM sizes of the two spots, the emission angle of the VCSEL can be determined to be 5.7°.

3. Alignment consideration

Several factors affect the packaging of an optical interconnection device when integrated with source lasers and photodetectors. Among others, the most important ones are lateral misalignment, angular misalignment, wavelength instability, and divergence of spot size.

3.1 Lateral and angular misalignments

Lateral misalignment means the misalignment of the device position due to the inaccuracy in its x-y directions. Lateral misalignment can be divided into absolute and relative misalignments. With current self-aligned flip-chip solder bump bonding process [9], the absolute lateral misalignment can be controlled with an accuracy of ~1 μm. Once coupled into the substrate, the signal beam travels towards the photodetector, a lateral misalignment in the clock laser results in an equivalued spatial shift of the output signal beam.

The influence of the angular misalignment on the lateral misalignment arises from the phase mismatch between the input signal beam and the grating vector when the incident angle deviates from the Bragg angle. Fig. 5 shows the phase-matching condition of a hologram for surface-normal coupling. A variation of the angle of the input light beam will lead to a spatial shift of the fan-out beam on the device surface of

$$\Delta L = \frac{[\tan(\gamma + \Delta\gamma) - \tan\gamma]}{\tan\gamma} L \qquad (1)$$

This relation is schematically shown in Fig. 6 for the optical backplane with nine-board interconnect. In our calculation, we have assumed the wavelength of the source laser as λ = 850nm, n = 1.512 (polymer waveguide), $\theta = 0°$ (surface-normal), $\gamma = 45°$ and L is taken as the longest distance.

We see from Fig. 6 that within a small angular misalignment of the input light beam, ΔL changes linearly with $\Delta\theta$. However, Fig. 6 also shows that the control of the angular alignment is not an easy task. To keep the spatial shift of the output signal beam below an error range of $\pm$ 50 μm (for a Silicon APD, typical size of the active area is on the order of ~100 μm at 1 GHz), the angular misalignment should be within $\pm\ 0.1°$. For the optical backplane device with substrate thickness of 0.125", the distance between the first and the last output channel is 5.08 cm, the situation is even worse. This stringent requirement is significantly relaxed by applying gradient index lens (GRIN) or microlens.

3.2 Wavelength Instability

Variation of lasing wavelength from the design value influences the spatial shift of the output signal beam via the same mechanism as does the angular misalignment. In fact, this mechanism has been used in the design of a wavelength division demultiplexing (WDDM) device[11]. The theory behind this mechanism is that a deviation in wavelength of the input signal beam will lead to an angular deviation of the diffracted beam from the Bragg angle. This produces as the spatial shift of the output beam.

The variation of spatial position of a fan-out beam on the device surface is linearly dependent on the shift of wavelength of a signal beam. Generally, the emission line width from VCSELs can be less than 1 A°. The misalignment due to this spectral width factor can thus be ignored when considering that the normal size of the photodetector active area is on the order of ~100 μm. For a VCSEL with three quantum well (QW) InGaAs/GaAs active region, the lasing wavelength varies with temperature in a rate of ~0.5 A°/K. To maintain a spatial shift within $\pm$ 50 μm, the allowable temperature variation is $\pm$ 5.8 K, which is within the limit of the contemporary optoelectronic temperature stability control level.

For the VCSELs, the active light emitting window has a diameter of 5 μm and a lasing divergence angle of $5°$. After propagating 2.2 cm in the substrate, the spot size becomes 615 μm. This enlargement of the spot size renders the photodetector impossible to respond in comparison with the ~100 μm size of the detector active region for an 1 Gbit/sec system. To make the system practical, precise beam profile manipulation is required. Here we introduce GRIN (gradient index) lenses into our system. A 0.25 pitch GRIN lens is suitable for our application. After the signal beam from the VCSEL travels through the GRIN lens, it will get collimated. Theoretically, as long as the collimated beam remains surface-normally incident onto the GRIN lens at the output end, it will be focused into a diffraction-limited spot. If the input signal beam has a misalignment $\Delta\theta$ in its input angle, then the ray matrix gives the spot shift at the focusing end as $\Delta r = \dfrac{\Delta\theta}{N_0\sqrt{A}}$, where N_0 is the refractive index on the central axis of the GRIN lens, $\sqrt{A}$ is the index gradient constant. At $\lambda = 0.85$ μm, N_0=1.6457 and $\sqrt{A}$=0.423, with a misaligned angle of 2 degrees, the shift of the output spot from the central axis of the GRIN lens is $\Delta r \approx 50\ \mu m$, while without the GRIN lens, this same angular misalignment would give ~1 mm.

4. Power requirement of optical backplane

The required laser power for an optical interconnection device is determined by the efficiency of the input and output couplers and the receiver sensitivity. For our optical backplane device, we assume the efficiency of an output channel is η. Without considering the reflection and propagation losses inside the substrate, we get the relationship between the input and output power as $P_{out} = \eta\ (1\text{-}R)\ P_{in}$, where R is the reflectivity of the input grating coupler. Without any anti-reflection coating mechanism, experiments show R≈ 11%. With our experiment, the minimum output efficiency of the optical backplane for all input configurations is 1.57%[3], which together with the sensitivity of the APDs gives a minimum power input of the backplane of 3.0 μW. The maximum input of the backplane can be determined by the output channel with the largest efficiency for all input configurations when the receiver at the output port is in saturation. With a sensitivity of 0.04 μW and an average dynamic range of 30 dB, the maximum power of a signal that can be received by a receiver without distortion is 40 μW. With our experiment, the maximum output efficiency of the performance optimized optical backplane is 74.5%[3], so the maximum required laser power input is 60 μW. Thus, the allowable range of the input laser power for our optimized optical backplane is 3.0 μW-60 μW, which can be easily achieved using state of the art VCSEL technology.

5. Data transfer integrity measurement

Except for power requirement, the performance of an optical interconnection device is characterized by its bandwidth, and its data transmission integrity. In this section, we demonstrate the experimental performance of our devices in these aspects.

5.1 System Bandwidth and Signal Response Measurements

One of the advantages of optical interconnects over traditional electrical circuits is the much wider bandwidth of optics. Bandwidth, which determines the highest speed the information can be transferred without distortion, was measured in our experiment by the frequency response of the device. In our experimental setup, a laser beam of 4.3 W at a wavelength of 514.6 nm from an Argon laser (Coherent I-90 Plus) is used to pump a Clark-MXR Ti:Sapphire Mode-Locked laser whose output is then fed into the optical interconnection device. A Clark-MXR Auto-Correlator (AC-150) analyzes the output signal from the device and sends the results to an ODL Data Acquisition System. The output measurement from the mode-locked laser showed that the demonstrated pulse has a speed of 150 fs with a power of 0.4 W centered at 850 nm.

After correlation, the profiles of the pulse signal with and without the interconnection device can be obtained. The propagation distance of the pulse inside the device is 5.08 cm, which is equivalent to the propagation from the 1st to the 9th channel of our optical backplane device. Due to the dispersion of the backplane material, the pulse from the backplane experiences a broadening effect relative to the reference pulse.

By making a fast Fourier transform (FFT) of the output pulse from time domain to frequency domain, the frequency response of the optical interconnection device can be automatically determined when compared with the FFT result of the reference pulse which is directly coupled into the correlator from free space. Fig. 7 shows the FFT results for the reference and the device output pulses. It is clear from Fig. 7 that a 2.5 THz (2,500 GHz) bandwidth is expected out of the optical interconnection system.

5.2 Eye Diagram Measurements

By overlaying sweeps of different segments of a long data stream driven by a master clock, we can get an eye diagram on the screen of a storage oscilloscope (analog or digital). In communication industries, the eye diagram is used to observe and analyze the performance of circuits that drive the transfer of digital data streams. Ideally, when many traces of randomly generated data series have been overlaid, positive- and negative-going pulses are superimposed on each other, a picture of a rectangular box results. In practice, especially when the displayed signal has traversed an imperfect communications channel, the traces do not lie perfectly atop one another, and a classic eye pattern results.

In order to measure the eye diagram of our optical interconnection devices, the random bit pattern from a 3 GHz Pulse Generator (HP8133A) is used to current-modulate an 822 nm semiconductor laser transmitter (FOT-FP-820-1M/3G-5/125-0 from Lawrence Labs, Ltd.). After being collimated and passing through the device, the optical signal from the transmitter is focused onto a high-speed (1.5 GHz) PIN silicon photodiode (Hamamatsu S4753). The output of the receiver is then analyzed by a Digitizing Oscilloscope (HP54120A).

To demonstrate the performance of our device, eye diagrams at the speeds of 500 MHz, 1 GHz, and 1.5 GHz were measured with and without the device for comparison. The final experimental results of three cases in 5.08cm propagation are shown in Fig. 8 and 9. Much information can be gained from the measurement of the eye diagram. The horizontal dark areas of the display show the time-voltage combinations at which the signal spends most of its time, while the cross fainter areas correspond to less frequent (but possibly more troublesome) events. The clear, inside portion of the display is known as the eye. A very clean signal will have a large, clear eye, while a noisy, low-quality signal will have a smaller one. The eye can become completely closed if the data signal has a lot of timing jitter with respect to the master clock, if the pulse widths are incorrect, or if varying amounts of noise and attenuation cause the signal amplitude to vary excessively. By comparing the eye diagrams before (Fig. 8) and after (Fig. 9) the insertion of our optical interconnection device, we see that the signal noise is mainly from the test system, and the device contributes no noticeable distortion to the signal. Even up to data speeds as high as 1.5 GHz, our experiment shows very clear open eyes, both with and without the device.

6. Experimental demonstration of bi-directional optical backplane with multi-bus lines

6.1 Experimental demonstration

Fig. 10 shows the experimental results of the above proposed backplane with three bus lines (1-D). The separation between the two lines is 140μm, which corresponds to VCSEL #1 and #2 on the 1-D 32 VCSEL arrays of 140μm pitch. A further improvement in the performance of the backplane with multi-bus lines can be achieved by using 2-D VCSEL and photodetector arrays instead of 1-D, so that the real estate of the backplane can be effectively utilized. For collimating of the

laser beams, we used ¼ pitch GRIN lenses with a diameter of 1mm. This idea is demonstrated by the experimental results in Fig. 11, where the input/output configurations of the backplane with 4-bus lines but 2 by 2 are demonstrated.

6.2 Crosstalk analysis and S/N Ratio

Currently, the commercially available GRIN lenses have a minimum radius of 0.5mm. So in our experiment the minimum separation of the bus lines should be 1mm. But due to the crosstalk between the adjacent bus lines, this minimum separation should be justified according to the requirement of the Signal to Noise Ratio (SNR). Even with a collimating GRIN lens, because of the alignment error and the Gaussian beam effect, the crosstalk still needs to be studied.

If there are two adjacent receivers with a radius of R and at a distance of d in a polar coordinate system, we obtain the total noise collected by detector as

$$P_{noise} = 2\int_{d-R}^{d+R} \int_{-\arccos\frac{\rho^2+d^2-R^2}{2\rho d}}^{\arccos\frac{\rho^2+d^2-R^2}{2\rho d}} P\cdot \rho d\theta d\rho \tag{2}$$

where the factor 2 is due to the noise from the laser beam located at 2d site. For a Gaussian beam centered at the origin, its intensity distrbution is

$$P = P_0 e^{-2\frac{\rho^2}{w^2}} \tag{3}$$

By inserting intensity distribution into equation (2), we can have

$$P_{noise} = 4P_0\int_{d-R}^{d+R} e^{-2\frac{\rho^2}{w^2}} \arccos\frac{\rho^2+d^2-R^2}{2\rho d}d\rho \tag{4}$$

The signal intensity collected by each detector is

$$P_{signal} = \int_0^R P\cdot 2\pi\rho d\rho = \frac{\pi w^2}{2}P_0\left(1-e^{-2\frac{R^2}{w^2}}\right) \tag{5}$$

With above equations, we can calculate the signal to noise ratio S/N. The variations of the S/N with those of the radius of lens and beam waist were calculated numerically. The result of calculation is shown in Fig. 12 with the detector separation of 1.4mm and lens radius of 0.5mm. From this figure we see that for our experiment, in which the radius of lens is 0.5mm, crosstalk is negligible until beam waist reaches 1mm at which S/N≈15. Because of the alignment error of the collimating lens, the laser beam coming out of the lens is divergent. We see that for our backplane with a total length of 5.08 cm, the spreading of the laser beam is around 0.8 mm due to the beam divergence. So, the S/N ratio of our device is greater than 15. Similar calculation gives the relationship between the beam waist and the divergent angle for a propagation distance of 5.08 cm. We see from this that, to keep the S/N ratio greater than 15 (i.e., w≤1 mm), the divergent angle can be as high as 1°.

For the backplane with 2D VCSEL and photodetector arrays, if only crosstalk from nearest lasers are considered, the noise power can easily be obtained as

$$P_{noise} = 8P_0\left(\int_{d-R}^{d+R} e^{-2\frac{\rho^2}{w^2}} \arccos\frac{\rho^2+d^2-R^2}{2\rho d}d\rho + \int_{\sqrt{2}d-R}^{\sqrt{2}d+R} e^{-2\frac{\rho'^2}{w^2}} \arccos\frac{\rho'^2+2d^2-R^2}{2\sqrt{2}\rho' d}d\rho'\right) \tag{6}$$

The diagram of S/N versus beam waist (with R=0.5 mm) is shown in Fig. 13. From this figure, we see that for R=0.5 mm and d=1.4 mm, the S/N ratio is 15 when w≈ 0.85 mm. Also this show that with the same values of d, R and w, the S/N ratio is about half of the case with 1D arrays of VCSELs and photodetectors. So, the crosstalk from the VCSELs in the diagonal directions can be considered to be unimportant. This justifies our assumption of considering the crosstalk only from the nearest VCSELs.

For 2-D application, 8x8 VCSEL arrays with 250μm pitch are commercially available. But the beam propagation performance depends on the emitting spot radius of the VCSEL and focal length of lens array [12]. Fig. 14 shows beam diameter as function of the propagation distance with various focal length of lens. From this figure, if the possible choice of focal length of microlens is from 1.0 to 2.0mm, lens pitch could be around 500μm when total propagation distance for nine boards is 5.08cm. In the case of the 24cm of the propagation distance(3.0cm separation of each boards), the possible focal length of lens will be larger than 3mm for 1mm lens pitch. So another problem arises from the choice of microlens due to the

beam propagation performance. We can select various choice of lens pitch by considering the crosstalk, but large focal length of microlens are difficult to make and take longer to fabricate.

7. Summary

We characterized our bi-directional optical backplane for multi-boards interconnects from alignment, power requirement, and data transfer integrity. Both angular and wavelength instability-induced misalignment were discussed. By using collimating lens in our design, we showed that the alignment problem could be greatly relaxed. From the performance optimized output results, we calculated the allowable laser input power ranges for optical backplane, which turned out to be 3.0μW ~ 60μW for our optimized bi-directional optical backplane. Frequency response of our devices showed a bandwidth of 2.5 THz from its performance test. Eye diagrams up to 1.5GHz have been demonstrated with clear eyes.

Finally we further proposed and demonstrated performance enhanced bi-directional optical backplane with multi-bus lines. By employing VCSEL and photodetector arrays, we presented backplane with 1-D and 2-D bus lines, which greatly increase the bus aggregate bandwidth of the backplane. Since minimum pitch of VCEL array, which is the pitch for an acceptable output crosstalk, is seriously dependent of the total propagation distance and focal length of lens, minimum pitch for the 5.08cm propagation was 500μm with focal length of from 1mm to 2mm. Since longer propagation may cause more divergence of beam profile, we should consider proper choices of pitch and focal length for microlens array from the beam propagation performance.

Acknowledgments

This research is sponsored by DARPA, ONR, AFOSR, BMDO, Army Space and Missile Defense Command, 3M Foundation, Cray research, and the ATP program of the state of Texas. The authors would like to thank Dr. Brian Davies and Chunhe Zhao for their helpful recommendations.

Reference

[1] L. W. Shacklette, K. M. T. Stengel, L. Eldada, C. Xu, and J. T. Yardley, "Polymeric waveguides for optical backplanes," SPIE, **2467**, 107(1995).

[2] C. Sebillotte, "Holographic optical backplane for boards interconnection," SPIE: International Conference on Advances in Interconnection and Packaging, **1389**, 600(1990).

[3] S. Natarajan, C. Zhao, and R. T. Chen, "Bi-directional optical backplane bus for genera purpose multi-processor board to board optoelectronic interconnects," IEEE Journal of Lightwave Technology, **13**, 1031(1995).

[4] T. Sakano, T. Matsumoto, and K. Noguchi, "Three dimensional board-to-board free space optical interconnections and their application to the prototype multiprocessor: COSINE-III," Applied Optics, **34**, 1815(1995).

[5] A. Takai, T. Kato, S. Yamashita, S. Hanatani, Y. Motegi, K. Ito, H. Abe, and H. Kodera, "200-Mb/s/ch 100-m optical subsystem interconnections using 8 channel 1.3-mm laser diode arrays and single-mode fiber arrays," Journal of Lightwave Technology , **12**, 260(1994).

[6] T. Nagahori, M. Itoh, I. Watanabe, J. Hayashi, and H. Honmou, "150Mbit/s/ch 12- channel optical parallel interface using an LED and a PD array," Optics and Quantum Electronics, **24**, S479(1992).

[7] D. Vakhshoori, J. D. Wynn, and G. J. Zydzik, "8 x 18 top emitting independently addressable surface emitting laser arrays with uniform threshold current and low threshold voltage," Applied Physics Letters., **62**, 1718(1993).

[8] A. von Lehmen, C. Chang-Hasnain, J. Wullert, L. Carrion, N. Stoffel, L. Florez, and J. Harbison, "Independently addressable InGaAs/GaAs Vertical cavity surface emitting laser arrays," Electronics Letters , **27**, 583(1991).

[9] M. J. Wale and C. Edge, "Self-aligned flip-chip assembly of photonic devices with electrical and optical connections," IEEE Transactions on Components, Hybrids and Manufacturing Technology, **13**, 780(1990).

[10] H. Kogelnik, "Coupled wave theory for thick hologram gratings," The Bell System Technical Journal, **48**, 2909(1969).

[11] M. M. Li and Ray T. Chen, "Two-channel surface-normal wavelength division demultiplexer using substrate guided waves in conjunction with multiplexed waveguide holograms," Applied Physics Letter, **66**, 262(1995).

[12] K. Hirabayashi, T. Yamamoto and S. Hino, "Optical backplane with free-space optical interconnections using tunable beam deflectors and a mirror for bookshelf assembled terbit per second class asynchronous transfer mode switch", Opt. Eng. **37**(4), 1332(1998).

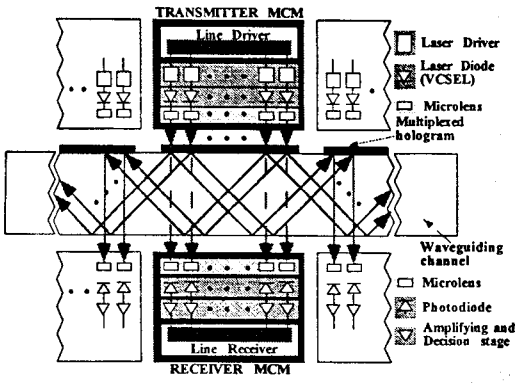

Fig. 1 Detailed diagram of waveguiding structure and transmitter and receiver modules of the proposed backplane with multi-bus lines.

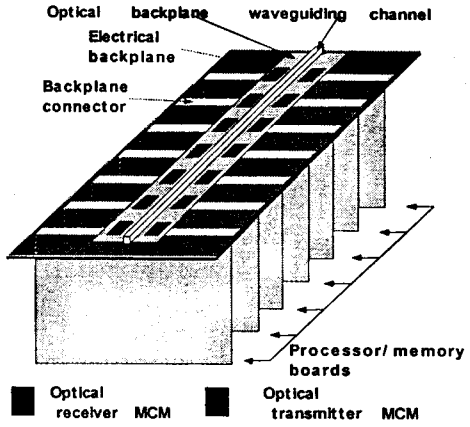

Fig.2 Overall architecture of the proposed backplane with multi-bus lines

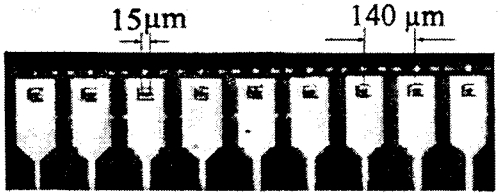

(a)

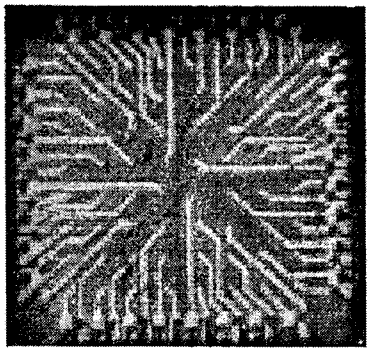

(b)

Fig. 3 VCSEL (a) 1x32, 140μm pitch 1-D array, (b) 8x8, 250μm pitch 2-D array

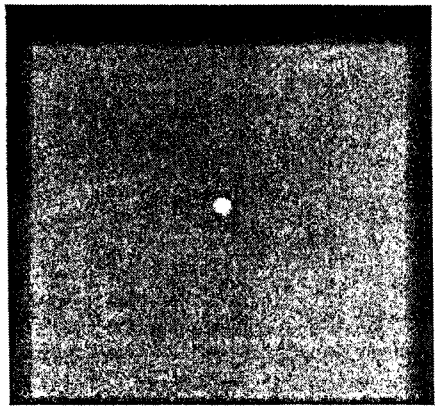

(a)

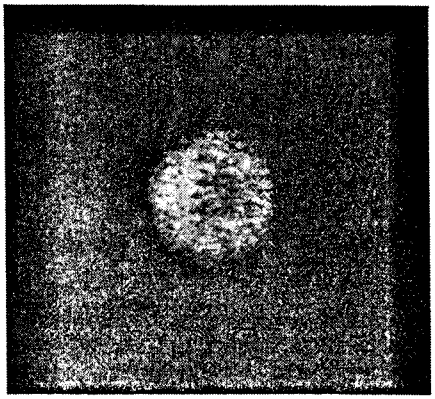

(b)

Fig. 4 Far-field profiles of the VCSEL output with (a) at ~1 mm from the emission window and the distance between (a) and (b) is 5 cm.

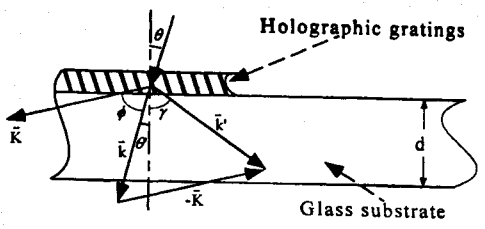

Fig. 5 Phase-matching diagram correlating the grating vector $\vec{K}$, the incident beam $\vec{k}$ and the diffracted beam $\vec{k}'$ for a slanted holographic grating element.

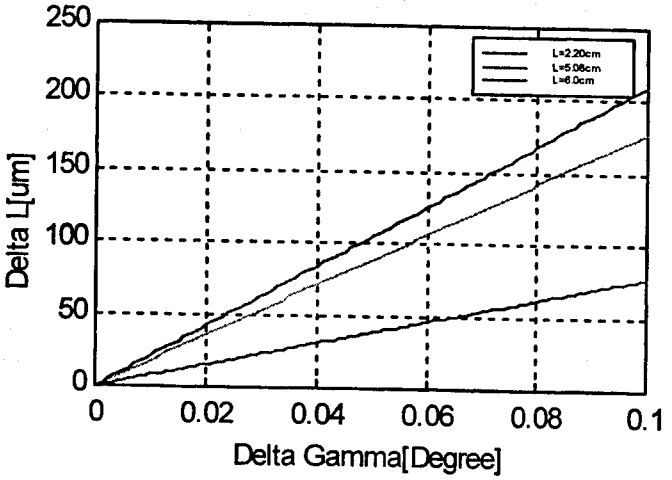

Fig. 6 Variation of spatial position of fan-out beam on the device surface with respect to the angular misalignment of the input signal beam.

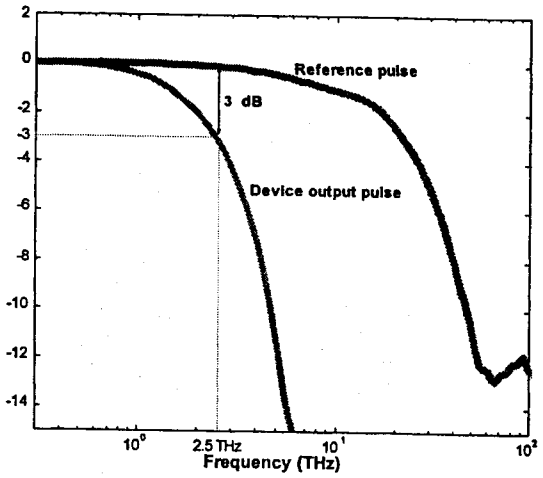

Fig. 7 FFT results of the pulses

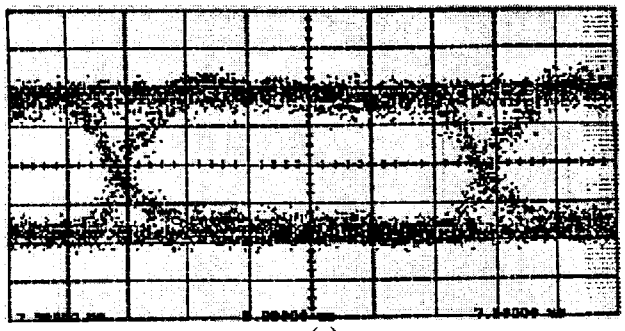

(a)

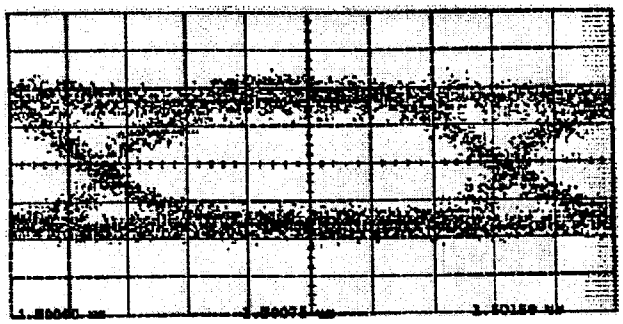

(b)

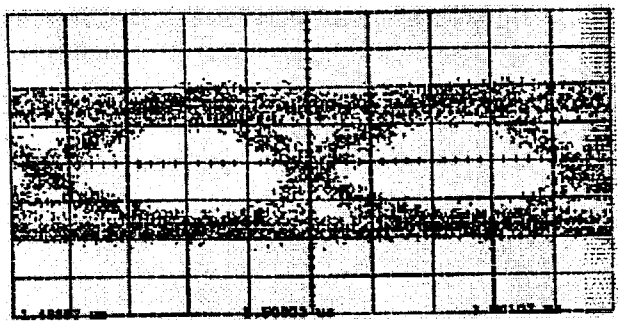

(c)

Fi g. 8 Eye diagrams of the system output as a function of data rate without the interconnection device. The laser modulation rates were (a) 500 MHz, (b) 1 GHz, and (c) 1.5 GHz.

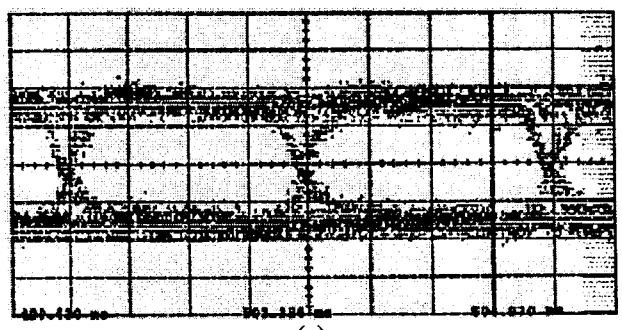

(a)

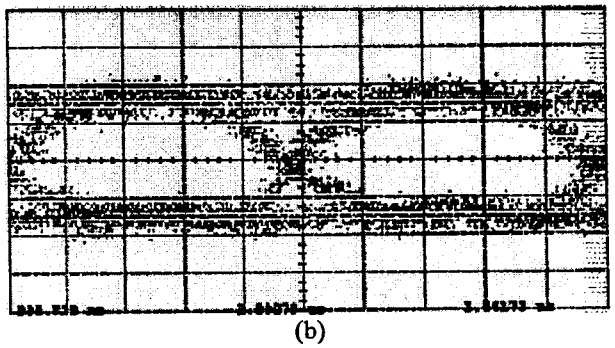

(b)

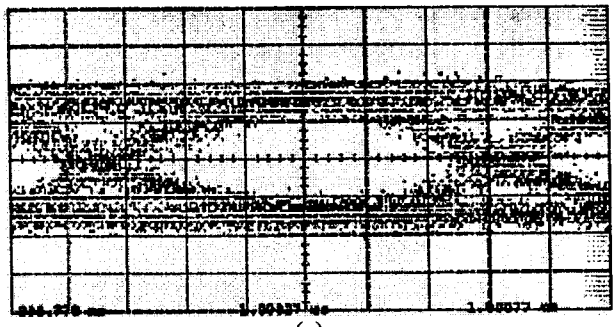

(c)

Fig. 9 Eye diagrams of the system output as a function of data rate with the interconnection device. The laser modulation rates were (a) 500 MHz, (b) 1 GHz, and (c) 1.5 GHz.

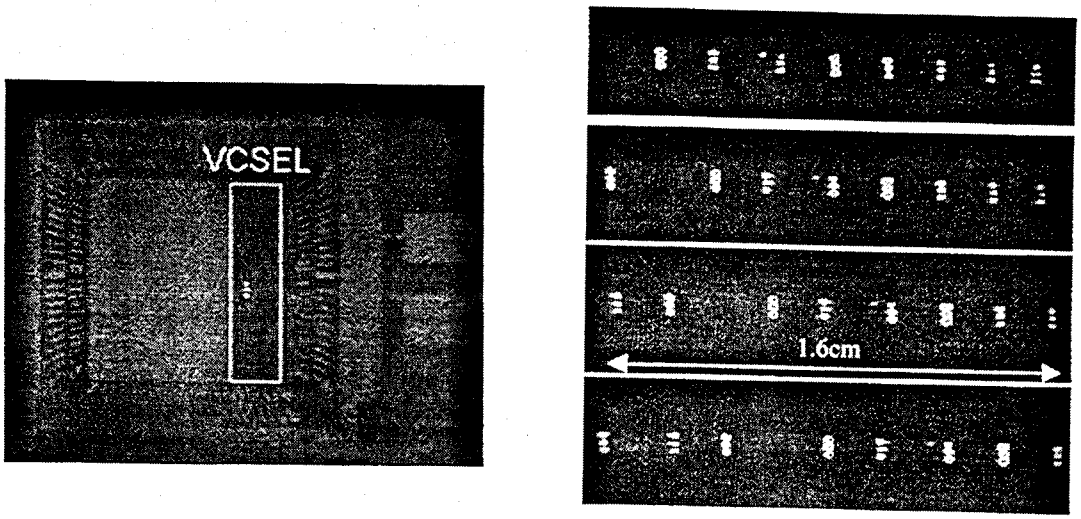

Fig. 10 Photograph of bi-directional optical backplane with 1D bus lines : 3 bus lines with 1st, 2nd, 3rd, and 4th channel functioning as the input couplers

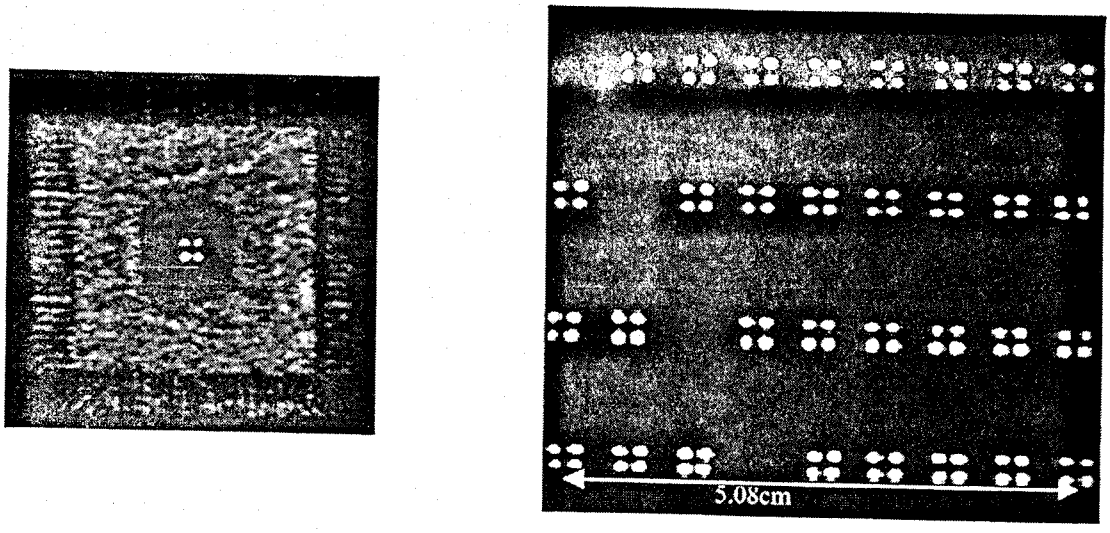

Fig. 11 Photograph of bi-directional optical backplane with 2D matrix(4 for this case) bus lines

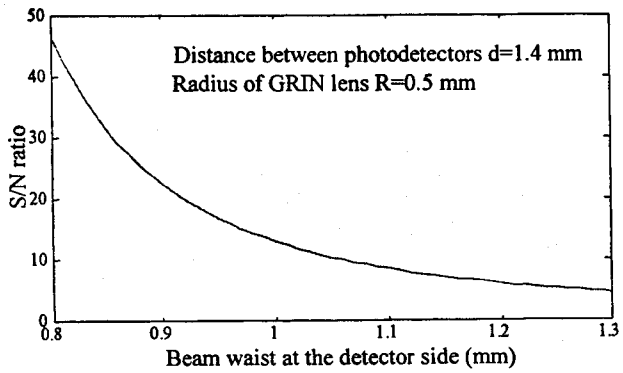

Fig. 12 Variation of S/N with that of the beam waist (with R=0.5 mm) for the backplane with 1-D arrays of VCSELs and detectors.

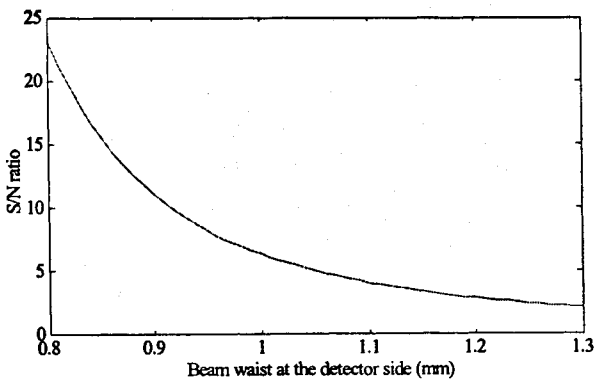

Fig. 13 Variation of S/N with that of the beam waist (with R=0.5 mm) for the backplane with 2-D arrays of VCSELs and detectors

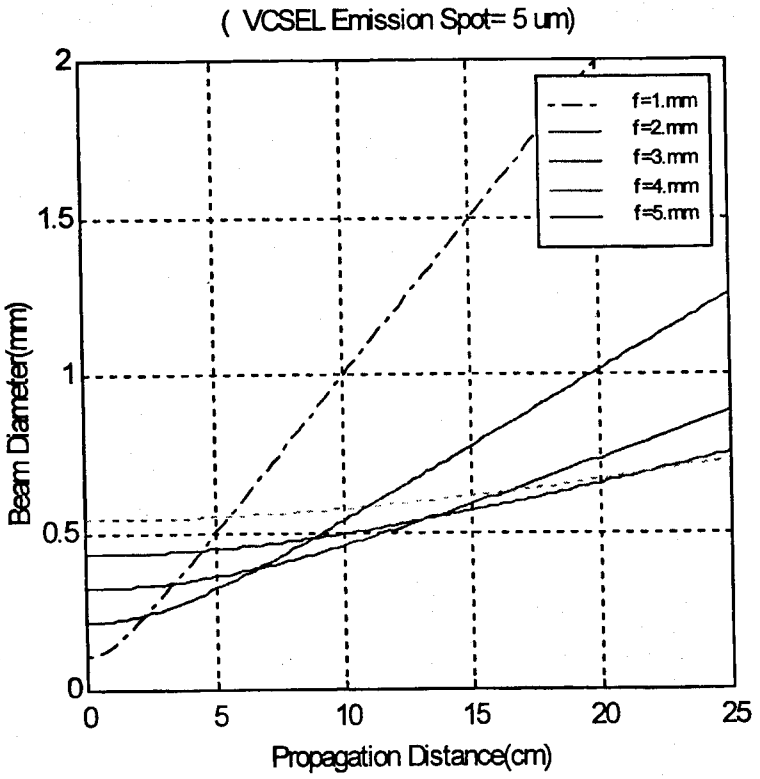

Fig. 14 Beam propagation performance depending on the focal length of lens